Available online at www.sciencedirect.com
ScienceDirect
International Journal of Multiphase Flow 34 (2008) 447–460
International Journal of Multiphase Flow
www.elsevier.com/locate/ijmulflow

Analysis of the unconventional behavior of oil relative permeability during depletion tests of gas-saturated heavy oils

Maria C. Bravo [a,*], Mariela Araujo [b]

[a] Applied Research Center, Florida International University, 10555 WFlager Street, EC 2100, Miami, FL 33174, USA
[b] Shell E&P Co, Two Shell Plaza 2225A, 777 Walker Street, Houston, TX 77002, USA

Received 15 May 2007; received in revised form 5 October 2007

Abstract

The description of two-phase flow in porous media is traditionally based on Darcy's equation. Accordingly, effective permeabilities to each phase are expected to be smaller than absolute permeabilities, and also they determine each phase mobility. A typical behaviors such as oil relative permeabilities values larger than one, can be obtained during depressurization experiments of heavy oil saturated porous media when the data is analyzed under the conventional Darcean approach. Such an unconventional behavior is physically possible considering that the Darcean approach disregard several flow sources such as viscous coupling derived from the momentum transfer between the phases. Oil relative permeabilities larger than one, which actually are apparent values, could represent one of the most convincing evidence of the role of viscous coupling on two-phase flow in porous media. In this paper we present experimental indication of such unconventional behavior and show how it can be properly understood when taking into account the viscous coupling contribution on each phase mobility. Pore network simulations are used to complement the analysis and evaluate the effect of the capillary number on the transport parameters involved in the generalized flow equations.

Keywords: Relative permeability; Bubble dynamics; Two-phase flow; Viscous coupling; Porous media; Pore network simulation

1. Introduction

The macroscopic description of the flow of two immiscible fluids in porous media has been intensely studied in recent years in attention to the variety of scientific and engineering problems that require its detailed comprehension (Chen and Keh, 1998; Karpyn et al., 2007). Particularly in the oil industry, the modeling of the transport of two and three fluid phases is a key element in the prediction of production resulting from any recovery process going from primary to enhanced oil recovery of subsurface fluids (Dullien, 1992; Sahimi, 1993; Vizika et al., 1994). The interplay between the microscopic governing physics and the macroscopic behavior is one of the most important and complex issues relative to this endeavor since the small-scale physics is represented by average parameters in mesoscopic differential equations (Hilfer, 1996).

Relative permeability, one of the mesoscopic parameters involved in the description of the simultaneous flow of fluids in porous media, represents the fraction of the permeability of the porous medium corresponding to each phase (Donaldson and Tiab, 2003). In other words, it is the effective permeability to a particular phase divided by the porous medium permeability. This concept emerges from the extension of Darcy's equation from single-phase flow to two-phase flow and by definition, it is not expected to be larger than one (Corey, 1994).

The validity of Darcy's equation for two-phase flow is based on the fulfillment of some conditions commonly assumed, among which are that a unique set of flow paths exist for each saturation value and when either fluid

* Corresponding author. Tel.: +1 305 348 6010; fax: +1 305 348 6011.
E-mail addresses: bravom@fiu.edu (M.C. Bravo), Mariela.Araujo@shell.com (M. Araujo).

0301-9322/$ - see front matter © 2007 Elsevier Ltd. All rights reserved.
doi:10.1016/j.ijmultiphaseflow.2007.11.003

becomes discontinuous in the flow domain, no flow of this fluid takes place (Bear, 1988; Whitaker, 1986a). The last assumption does not consider that momentum transfer can induce movement from the continuous phase to the discontinuous phase, a phenomenon well captured in the generalized flow equations derived by Whitaker (1986b), Kalaydjian (1987, 1990). Thus, relative permeability experimentally obtained through Darcy's equation, is anchored to a physical interpretation that does not allow results such as relative permeability values larger than one.

We gathered a number of experiments that evidence that relative permeabilities values larger than one can be obtained under particular flow conditions (Tang and Firoozabadi, 2003; Maini and Sarma, 1994; Andarcia et al., 2002). These experiments were done to improve the understanding of how the depressurization process of saturated heavy oil (with dissolved gas) in a porous medium would impact the oil and gas production rate. Even though in all cases the authors overlook "oil relative permeability values larger than one" obtained from their experiments, it is clear that a careful analysis of such unconventional results would warrant an improved understanding of the 'dynamics' of 'foamy oil' (Chen, 2006).

In this paper we perform a detailed analysis of reported experimental data by assessing their basic experimental conditions, and the evolution of the flow regime during the tests. The analysis evidences the consequences that a conventional interpretation of experiments has on the description of bubbly-oil flow through porous media and its predictions.

We demonstrated in a previous work (Bravo et al., 2007) that relative permeabilities larger than one can be obtained due to the contribution of momentum transfer between two-phases by explicitly considering the generalized flow equations with a viscous coupling term. In this work we review the dynamic conditions under which this theoretical result could explain the aforementioned experimental findings. We perform pore network simulations to determine the impact of the flow regime and the oil viscosity on the unconventional behavior of relative permeability.

2. Analysis of experiments

2.1. Characteristics of experiments

Experiments to study the dynamics of two-phase flow that occurs during depletion of heavy oil reservoirs intend to reproduce at lab scale the real flow at reservoir conditions. Usually, cylindrical flow symmetry is assumed at field scale and consequently the flow rate is proportional to the inverse distance to a well. Experimentalists consider very difficult to reproduce this geometry in the lab and instead they work in a lineal geometry.

Fig. 1 illustrates the experimental setup used by Tang and Firoozabadi (2003) to study depressurization of saturated heavy oil in porous media. This setup can be considered standard for this type of experiments. The most

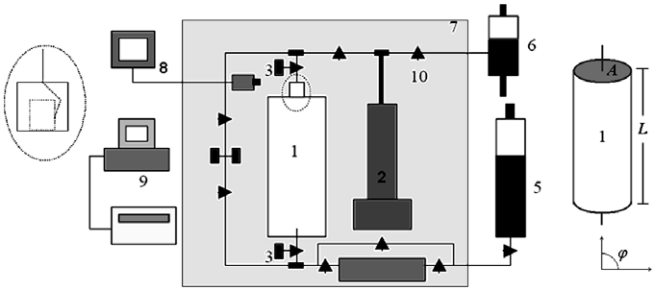

Fig. 1. Schematic of experimental design. 1 – core-holder; 2 – pump; 3 – pressure transducers; 5 – high pressure cylinder; 6 – oil/gas separator; 7 – temperature controlled camera; 8 – TV monitoring system; 9 – computer; 10 – valves. Adapted from Tang and Firoozabadi (2003).

relevant aspects that vary among the different experimental settings reported by different authors are the angle between the axial direction of the core-holder and the gravity acceleration direction (φ), the sample dimensions (Length, L and cross sectional area, A), the transparency of the core-holder and the number of pressure transducers placed along it. The sample is typically a core plug or a sandpack with a specific saturation condition.

In general terms the experimental procedure consists in flooding the core or sandpack with oil until achieving steady state in pressure and flow conditions, then the system is opened for production by blowing down the pressure through the outlet end, while no flow is allowed through the inlet. Notice that this procedure is different from the one followed in external gas drive tests and it is more representative of the internal gas drive production mechanism. Measurements are performed when a quasi-stationary state is reached, which allows considering a nearly constant pressure gradient along the sample.

2.1.1. Experiment by Tang and Firoozabadi

In Tang and Firoozabadi experiment, a saturated pressurized sandpack is submitted to depressurization, which is initiated at a pressure of 4915.9 kPa. Initially, the depletion test occurs at 2 cm^3/day. When an expansion volume, $\Delta V = 50$ cm^3, is reached, the rate is increased to 3 cm^3/day and from $\Delta V = 75$ cm^3 to the end of the test, the rate is fixed to 4 cm^3/day. When the gas begins to break through, the gas and unsaturated oil production are measured with an ISCO pump and the gas/oil separator (the first 6 cm^3 were measured in the graduated window located at the top of the core-holder). The fluids and sandpack properties relative to this experiment are given in Table 1. The oil volume factor is considered equal to one and consequently, the produced gas volume is calculated from the difference between the expansion volume (read in the pump) and the produced oil volume. Gas and oil production are measured every 0.01 pore volumes (PV) and the pressure and differential of pressure are automatically recorded every minute in the computer. Authors do not make reference to the change of oil viscosity with pressure during the test, and in fact they assumed a constant viscosity in their

Table 1
Saturated oil and sandpack properties corresponding to the experiments: Tang and Firoozabadi (2003), Maini and Sarma (1994) and Andarcia et al. (2002)

	Tang and Firoozabadi (2003)	Maini and Sarma (1994)	Andarcia et al. (2002)	
			2% Clay	5% Clay
Oil density (ρ_o), kg/m^3	980	968	1013	1013
Viscosity (μ_{ob}), Pa s	9.20	3.01	2.00	2.00
Bubble point pressure (P_b), kPa	2530.4	4826.3	7549.8	7549.8
Gas/oil initial ratio (Rs_i), vol/vol	6.5	14.8	18.7	18.7
Core-holder angle (φ), Rad	$\pi/2$	0	0	0
Core-holder external wall	Clear	Opaque	Opaque	Opaque
Length (L), m	0.536	2	0.50	0.50
Area (A), cm^2	31.65	16.1	23.75	23.75
Sand	Ottawa	Ottawa	Synthetic	Synthetic
Porosity (ϕ), %	35.6	33	41	39
Permeability (k), Darcy or $\times 10^{-12}$ m^2	13.7	3.5	3.48	1.78
Grain diameter (d), μm	212–355	74–105	180	92
Initial water saturation (Sw_i), %	0	2	7	9

calculations. This assumption may introduce significant errors in the estimation of oil relative permeabilities.

2.1.2. Experiment by Maini and Sarma

A sandpack, 98% filled with saturated oil, was depressurized by blowing down the pressure at the outlet end (P_{out}) to the atmospheric value. The experimental setup is similar to the one shown in Fig. 1, but in this case five pressure transducers were located every 40 cm along the core in order to monitor the pressure gradient. Fluids properties and other data corresponding to this experiment are given in Table 1. The authors reported the unsaturated oil viscosity as 8.580 Pa s.

2.1.3. Experiment by Andarcia et al.

The sandpack was flooded with saturated oil. Two experiments were performed, one for sand with 2% of clay (Kaolin) and the other with 5%. The sandpack was depleted from an initial pressure of 8273.7 kPa. The total production rate at the outlet was 0.66 cm^3/h, while the inlet was kept closed during the whole test. Relevant properties of fluids and sandpack are offered in Table 1. In this case no reference is made to the variation of oil viscosity with pressure.

2.2. Differential pressure. Measured vs. average macroscopic value

The pressure measured in experiments, when the gas phase is in the form of bubbles, may be different from the macroscopic pressure explicitly appearing in the flow equations derived by Kalaydjian through the principles of irreversible thermodynamics or by Whitaker through the method of volume averaging. Both approaches treat the two-phase flow on a macroscopic scale under a local equilibrium assumption. This means that they describe the fluid motion at the level of locally averaged variables so that, for example, even when there is a density gradient in the system, at any position (x,y,z), a local density value, $\rho(x,y,z)$, can be defined. In principle, different types of averaging may be used to determine the ρ value. According to spatial averaging, the density at (x,y,z) is defined as the ratio of mass to volume for a sphere centered at this point, such that it is large enough to include large number of particles (so that density fluctuations can be neglected) and small compared to the macroscopic scale (Bear, 1988). On the other hand, if an ensemble averaging is used $\rho(x,y,z)$, is the arithmetic mean of the actual density of the fluid occupying the point (x,y,z) for each of a large amount of macroscopically equivalent systems (Jackson, 2000). Similar definitions apply to any other measurable parameters like the pressure.

Kalaydjian's equations are not formally tied to local spatial averages and in principle other procedures of averaging, such as time average and/or ensemble average could be considered to get macroscopic quantities. However, from the description of the experiments in the previous section, it can be anticipated that in depressurization experiments the local spatial average is closer to the quantities derived from the physical process of measurement. To illustrate this, consider for example, the pressure. From the point of view of time-averaging, the measured pressure will correspond to a time averaged pressure if the measurement were performed during a period of time sufficiently large to sample all of the possible pressure values; however, this is not the case in these experiments. On the other hand, the ensemble average is not expected to correspond to the measured pressure either, since no sampling over a set of macroscopically equivalent systems is carried out in the previously described experiments.

Local spatial average over an averaging volume representative of the measurement window is the method of averaging that generates a pressure closer to that obtained from depressurization experiments and only if the ergodicity hypothesis can be demonstrated both, spatial and ensemble averages will be the same (Jackson, 2000). In the depressurization experiments, as in the case of steadily bubbling fluidized bed studied by Jackson (2000), these two

averages could be very different, given that phenomena like bubbles nucleation, growth, coalescence and breakup may be irreproducible by manipulating the macroscopic variables. In other words, the flow could be extremely sensitive to the initial and boundary conditions in depressurization experiments, and consequently an independent observation of the system, like performed in these experiments, would not be even a sample of the ensemble. Drew and Passman (1999) and Jackson (2000), though with different objectives, discussed well the difficulty of getting an ensemble average in actual measurements where the flow is sensitive to small changes in the initial conditions, boundary conditions and the sources terms.

On the other hand, the generalized flow equations derived by Whitaker are subordinated to the basic requirements of the application of a continuum approach to porous media (Bachmat and Bear, 1986; Bear, 1988) and the use of the average volumetric theorem may or may not be valid depending on the bubble size evolution and its distribution, since it might not be possible to even define a representative elemental volume (REV).

To apply such a continuum description, average values, calculated on a REV, should be independent of its dimensions and they and their derivatives should be continuous functions of time and space. Fig. 2 illustrates an idealization of a porous medium saturated with oil and gas (bubbles). Fig. 2a shows uniformly distributed gas bubbles where a REV can be defined, whereas Fig. 2b shows a non-uniform bubble distribution, where a REV can not be defined because the average values will depend on the dimensions of the volume (for example, the average density of the gas phase varies depending on what volume V_1 or V_2, is used in Fig. 2b) and also the continuity of the derivatives to first and second orders are not guaranteed. Increasing the REV dimensions is not an alternative, given that it may become comparable with the system characteristic dimension, L (as V_3 in Fig. 2b). Thus, when the bubbles are not uniformly distributed, the measured quantity does not correspond to the average parameter involved in the macroscopic flow equations based on the continuum approach, and a conceptual difficulty arises.

In a homogeneous porous medium, when the pressure drops below the bubble point pressure, bubble nucleation occurs randomly in space (Firoozabadi and Kashchiev, 1996; McDougall and Sorbie, 1999) and a uniform distribution of bubbles can be supported in many cases at the first stages of depletion. When the flow progresses, in addition to nucleation other phenomena such as bubble growth, coalescence and breakup determine the bubble distribution in the porous medium. Some visualization of heavy oil depressurization experiments have evidenced that nearly uniform bubble distributions are sustained during the entire test (Bora et al., 2000; Lago et al., 2002; Tang and Firoozabadi, 2003). In fact, in heavy oil, the coalescence of bubbles is disadvantaged due to the high viscosity of the oil (Joseph et al., 2002), nucleation on the contrary is advantaged (Bauget et al., 2001) and the competition among these phenomena and the bubble breakup finally results in the gas phase flowing as bubbles in heavy oil, while in light oil, a fingering pattern of the gas phase is observed for identical depletion conditions (Lago et al., 2002).

Returning to the previous discussion on the conditions for the use of the continuum approach, the experimental equivalent of the REV is the "measurement window", hence the uniformity condition and scale restrictions should be satisfied at the scale of this window. For an experimental setup as the one illustrated in Fig. 1, the area A, whose value for each experiment is given in Table 1, corresponds to the "measurement window" and the variations of differential pressure shown in Fig. 9 of Tang and Firoozabadi (2003) represents an example of the consequences of not satisfying the conditions required for a continuous description of the differential pressure. This is particularly

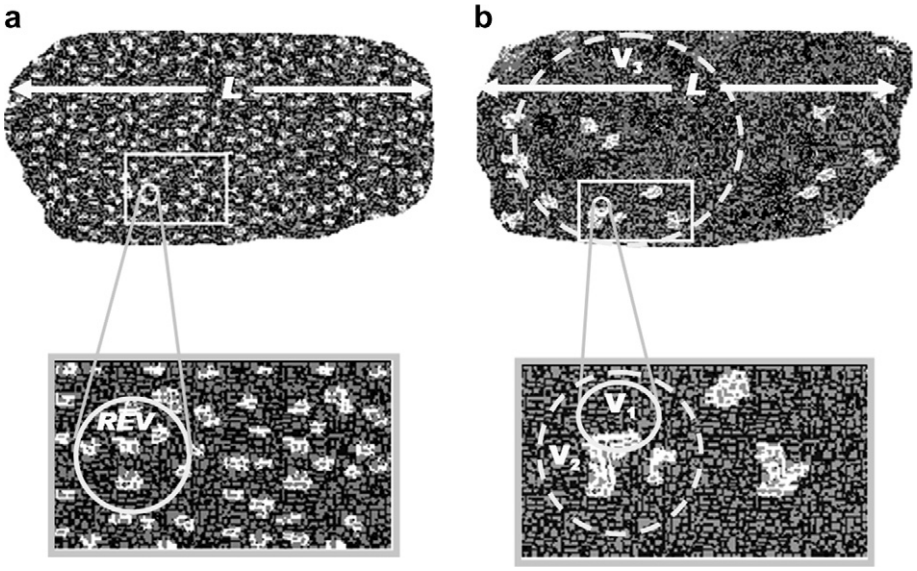

Fig. 2. Two different forms of bubbles distribution. (a) Uniform and (b) non-uniform.

true, if other possible sources of fluctuations, such as inappropriate experimental setup and/or inaccuracy of the pressure transducer, can be ignored. Tang and Firoozabadi (2003) do not report such problems in their experiments, while Andarcia et al. (2002), attributed the fluctuations of differential pressure to variation of temperature and thus variation in the oil viscosity. Certainly, variation of viscosity due to a ±2 °C change of temperature could cause fluctuations in pressure drop as high as 30%; however, Tang and Firoozabadi (2003) reported that temperature is controlled in their experiment with an accuracy of ±0.1 °C. Also, they observed that once the first bubble appeared in the surface of the core-holder the differential pressure jumped from 0.5171 kPa (corresponding to single-phase flow) to 0.6895 kPa (for $\Delta V = 11.85\ \text{cm}^3$). The pressure at the outlet and the differential pressure begin to fluctuate after this point. Authors refer that for 70.01 cm^3 around 70% of the bubbles were connected. Fig. 10 of Tang and Firoozabadi (2003) evidences that such connectivity means the formation (via coalescence) of relatively large bubbles, which still are much smaller than the axial dimension of the sandpack. Thus, the fluctuations of pressure drop observed in Fig. 9 of Tang and Firoozabadi (2003) can result from the non-compliance of the conditions required for a continuous description due to intermittent presence of gas in the measurement window.

In principle, the macroscopic pressure drop is measured in the connected phase (oil at the beginning of the test) and it is given by the difference of oil hydrostatic pressures at outlet (P_{oOut}) and inlet (P_{oIn}) of the sandpack. With the progress of the Tang and Firoozabadi (2003)('s experiment) the gas bubbles appear and their dimension increase. If we define a critical bubble dimension as a bubble whose dimension is comparable with area A and such a bubble is considered at the measurement window when part of it is inside of the sand pack (in the porous space) and the other part outside (in the flow line) as illustrated in Fig. 3, the location of oil and gas bubbles with respect to the measurement window determines that four conditions may take place in the experiment. Considering that P_{o1} and P_g are the oil and gas hydrostatic microscopic pressures, the four conditions and their consequences for the measured differential pressure are:

(a) Oil at inlet and outlet of sand pack. This occurs initially, when there are not bubbles in the sandpack, or at later stages, if no bubbles with critical dimension are located in the measurement window by the time of pressure measurement. In this case, the differential pressure is $\Delta P_o = P_{oOut} - P_{oIn}$.
(b) Oil at inlet and bubble at outlet measurement window. If the bubble has critical dimensions, the differential pressure will suffer an abrupt increase to represent the difference, $(P_g - P_{o1}) + \Delta P_o$.
(c) Oil at outlet and bubble at inlet measurement window. If the bubble has critical dimensions, the differential pressure will suffer an abrupt decrease to represent the difference, $(P_{o1} - P_g) + \Delta P_o$.
(d) Bubbles, with critical dimensions, at the inlet and outlet of the measurement window at the moment of pressure detection. Considering that capillary pressure is the same at both sandpack's ends, as expected in homogeneous sandpacks, the obtained value would correspond to the microscopic differential pressure $\Delta P_o = P_{oOut} - P_{oIn}$. Notice that the critical dimension of a bubble is negligible with respect to the sandpack's dimension, L and if the bubble's dimension tend to be comparable with L, then $\Delta P_o \to 0$.

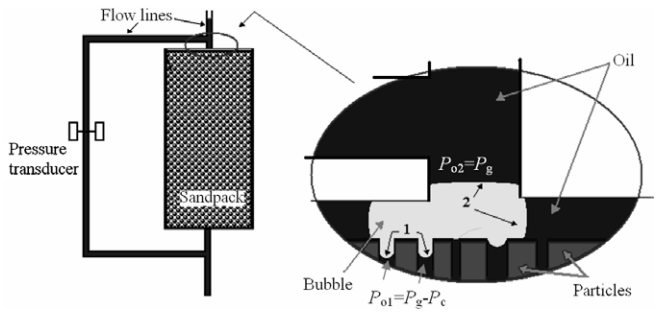

Fig. 3. Magnified visualization of a bubble at the "measurement window". Pores are represented by capillaries, with dimensions much larger than the real ones and solid particles are in correspondence with the pores capillary representation. Notice that at one side of the interface 1, the pressure is $P_{o1} = P_g - P_c$, while at the other side it is P_g.

The microscopic capillary pressure is related to the pore radius at the location of the interface. Thus for the type-1 interface illustrated in Fig. 3, the microscopic capillary pressure is given by $P_c = P_g - P_{o1}$ and the variation of differential pressure in case (b) and (c) corresponds to $P_c + \Delta P_o$ and $-P_c + \Delta P_o$, respectively. Therefore, fluctuations with amplitudes equal to $2P_c$ will be observed. For a bubble with critical dimension several interfaces will be located in different pores and considering that there is a distribution of pore sizes in the sandpack, a distribution of microscopic capillary pressure is expected. Thus, the maximum amplitude of the fluctuations in Fig. 9 of Tang and Firoozabadi (2003) should correspond to $2\langle P_c\rangle$, where $\langle P_c\rangle$ is the average or macroscopic capillary pressure in the sandpack.

Fig. 4 illustrates the amplitude of the fluctuations estimated from Fig. 9 of Tang and Firoozabadi (2003), as a function of the expansion volume and outlet pressure. The increasing trend of the fluctuations indicates an increase of capillary pressure with a decrease in P. In this experiment a layer of 1.5 cm of coarse sand, with grain size of 600–800 μm was placed at the top of the sandpack to prevent gas holdup under a stainless steel screen with an opening of 425 μm. Thus, in the earliest stages of fluctuations, the bubbles are mostly sampling the porous space of this layer, while at later stages they will be sampling the porous space of the sandpack. A transition region, between the two porous spaces is expected to be apparent as indicated by the smooth increase of the magnitude of

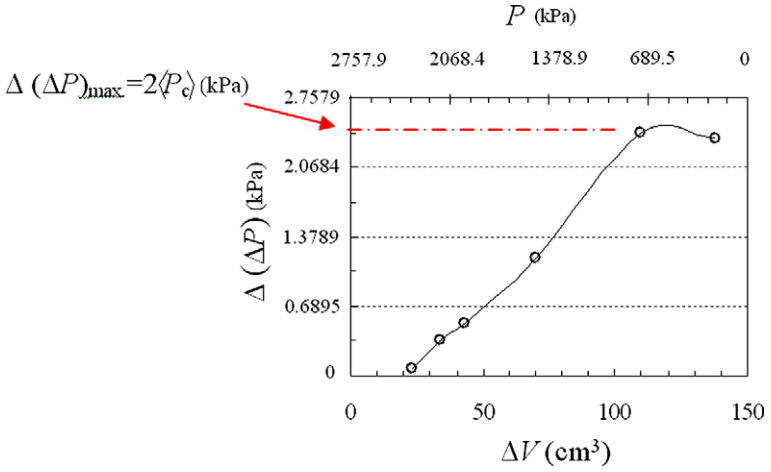

Fig. 4. Amplitude of differential pressure fluctuations, obtained from Fig. 9 of Tang and Firoozabadi (2003), vs. the expansion volume and pressure at outlet.

the fluctuations observed in Fig. 4. The fluctuations reach a maximum value, which in principle would remain approximately constant for subsequent stages of the experiment unless bubbles dimensions become comparable with the sandpack dimension L; however, the beginning of declination of the amplitude observed in Fig. 4, from $\Delta V = 110\ \mathrm{cm}^3$, indicates that these events started to occur.

According to the equation of Young and Laplace, for the cases of a spherical interface of radius a, inside of a capillary of radius r, the macroscopic capillary pressure is given by (Lyklema, 1991)

$$\langle P_c \rangle = 2\left\langle \frac{\sigma}{a} \right\rangle = 2\left\langle \frac{\sigma}{r}\cos\theta \right\rangle \cong 2\frac{\langle\sigma\rangle}{\langle r\rangle}\langle\cos\theta\rangle, \tag{1}$$

where θ is the contact angle and the angular brackets indicate average values. The last equality on the right of Eq. 1, is an approximation that assumes narrow distributions of σ, θ and r in the sandpack. Given the properties of the Ottawa sand used in the Tang and Firoozabadi (2003) experiment, we consider that this is an acceptable approximation for the current study.

Fig. 4 and the previous analysis indicates that $2\langle P_c \rangle \cong 0.35$ psi. In addition, the oil-wet condition implies that $\cos\theta$ values are in the range from 0.8 to 1, therefore $\langle\cos\theta\rangle = 0.9$ can be considered. On the other hand, since Ottawa sand is typically formed by rounded grains, the average pore radius can be estimated according to the level of packing of the sandpack. For example, for a cubic packing (in which each sphere sits directly on the crest of another sphere) the pore radius would be around 0.4 times the radius of the particles, while for rhombohedral packing (the spheres lie in the hollows formed by two adjacent spheres) this number is reduced to 0.15. We consider that most of larger and smaller pores are associated to the cubic and rhombohedral packings, respectively. From Table 1, we estimate an average grain radius of 141 μm and according to the packing level we infer that pores radii are between 56 μm (for cubic packing) and 21 μm (for rhombohedral packing). According to the porosity value of the sandpack (Perunicic and Babin, 2001) we may consider an intermediate packing and consequently $\langle r \rangle = 38$ μm.

Substituting the previous average values into Eq. 1, we estimate the average oil–methane interfacial tension to be around 41 mN/m. This is a realistic value for heavy oil–methane, considering that reported values are in the range from 20 to 45 mN/m (Lara, 1998). This calculation was helpful to verify that the maximum amplitude of the fluctuations corresponds to $2\langle P_c \rangle$; however, we suggest caution when using the approximations related to the last equality on the right of Eq. (1), in cases where more accurate estimations are needed.

The previous analysis indicates that the physical meaning of the experimentally obtained pressure and the macroscopic pressure could be different in conditions where bubble nucleation, growing, coalescence and breaking occur during the flow process. Other depressurization experiments have shown similar fluctuating behavior of the experimental pressure (Andarcia et al., 2002; Tang et al., 2006); but the conceptual problem involved has not been addressed. Tang and Firoozabadi (2003) assumed that an average curve corresponds to the macroscopic differential pressure involved in the flow equations, which is not necessarily true. Notice that if the four cases discussed above have a probability of occurrence f_i, with i varying from 1 to 4 for cases (a) to (d), respectively and assuming $\sum_{i=1}^{4} f_i = 1$, the average curve considered by Tang and Firoozabadi (2003) corresponds to

$$\overline{\Delta P_o} = f_1(P_c + \Delta P_o) + f_2(-P_c + \Delta P_o) + f_3\Delta P_o + f_4\Delta P_o \tag{2}$$

where, it has been considered that $\Delta P_c = 0$, so $\Delta P_g = \Delta P_o$.

For the particular case where $f_1 = f_2 = f_3 = f_4$

$$\overline{\Delta P_o} = \frac{P_c + \Delta P_o - P_c + \Delta P_o + \Delta P_g + \Delta P_o}{4} = \langle \Delta P_o \rangle \tag{3}$$

which evidences that in this case the average curve proposed represents the macroscopic pressure gradient involved in the flow equations. However, if the probabilities of occurrence are different, which is possible for a non-uniform bubble distribution, the mentioned average curve does not correspond to the macroscopic pressure gradient. For instance, the particular situation where $f_1 = f_3 = f_4 = f$ and $f_2 = 10f$, Eq. (3) gives

$$\overline{\Delta P_o} = \langle \Delta P_o \rangle - \frac{9}{13} P_c \tag{4}$$

Thus, an average curve would be underestimating the macroscopic pressure drop by $9/13 P_c$.

2.3. Apparent oil relative permeability

In this section we present the apparent oil relative permeability curves obtained from data reported by three different experimental groups: Tang and Firoozabadi (2003), Maini and Sarma (1994) and Andarcia et al. (2002). The term "apparent" is given to the relative permeability value obtained from the conventional Darcean approach (Bravo et al., 2007). The saturated oil viscosity for each experiment is offered in Table 1 and the dependence of oil viscosity, μ, with pressure, P, for $P < P_b$, is considered to follow a Khan-type correlation (Khan et al., 1987):

$$\mu(P) = \mu_{ob} \exp[-a(P - P_b)] \tag{5}$$

where, the bubble pressure (P_b) and the oil viscosity at this pressure (μ_{ob}) are listed in Table 1 for each experiment here analyzed. For heavy oil, $a = 0.221695\ \mathrm{MPa}^{-1}$ as obtained through Maini and Sarma (1994).

Apparent oil relative permeabilities from Darcy's equation, are given by

$$kr_o^{ap} = \frac{\mu_o(P) l Q / n}{kA(\Delta P + \rho_o g L \sin\varphi)} \tag{6}$$

where Q is the volumetric flow rate at the outlet of the sandpack and $\Delta P/l$ is the pressure gradient along the sandpack length, l. The parameter n considers that the relation of $\Delta P/l$ with Q depends on how representative is Q of the average volumetric flow through the segment l. For Tang and Firoozabadi (2003) and Andarcia et al. (2002) experiments, $l = L$ and consequently $n = 2$. However, for Maini and Sarma (1994), the pressure gradient is known for six sandpack segments and consequently $l = L/6$. In this case we consider the pressure gradient corresponding to the segment closest to the outlet, hence $n = 1$. Table 1 presents the values of oil viscosity at bubble point pressure μ_{ob}, the sandpack length L, permeability k, area A, density ρ_o, and angle φ for each experiment.

Gas saturation was estimated (when not reported by the authors) by material balance

$$S_g = 1 - S_o \text{ with } S_o = \frac{\left(\frac{V_o(P_r,T_r)}{B_{oi}} - Q_{cum}\right) B_o}{V_p} \tag{7}$$

where, $V_o(P_r,T_r)$ is the oil volume in the sandpack at reservoir pressure and temperature, Q_{cum} is the cumulated oil production, B_o is the oil formation volume factor (oil volume at P, T divided by oil volume at standard conditions) and V_p is the porous volume.

The flow regime at which each experiment was done is very relevant to get an adequate physical understanding of the results. We estimate the capillary number for each experiment using:

$$Ca = \frac{(\Delta P + \rho_o g L \sin\varphi)/Np}{Pc} \tag{8}$$

where, ΔP is the difference $P_{in} - P_{out}$; ρ_o is the oil density, g is the gravity; φ is the axial angle with the normal to the gravity (see Fig. 1); N_p is the number of solid particles in a line parallel to the pressure gradient direction (estimated as L/d; with d as the particle diameter); and P_c is the capillary pressure, obtained from Eq. (1) considering $\theta = 0$, interfacial tension of 0.036 N/m and the pore radius is taken as $0.4d$.

Fig. 5 illustrates the evolution of the capillary number with gas saturation for each experiment. Notice that in Andarcia et al. (2002) and Tang and Firoozabadi (2003) experiments, the capillary number was around 10^{-3}, whereas in Maini and Sarma (1994) experiment this number was between 10^{-1} and 10^{-2} for the same range of gas saturation. Visualization of the bubbles dynamics in the Tang and Firoozabadi (2003) experiment indicates that capillary forces are not governing the flow dynamics. According to this and considering the similarity on dynamic conditions of the Andarcia et al. (2002) and Maini and Sarma (1994) experiments, we infer that these experiments were performed under a predominantly viscous flow regime. In the next section we analyze the dependence of the flow regime with the capillary number, calculated via Eq. (8), from pore network simulations.

Oil relative permeabilities obtained from Eq. (6) calculated using reported experimental data are depicted in

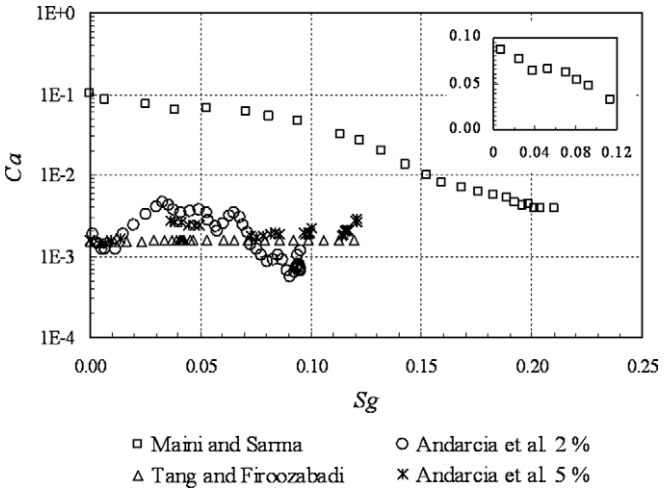

Fig. 5. Capillary number estimated from Eq. (8) for the analyzed experiments.

Fig. 6. Even though oil viscosity is pressure dependent we have obtained the relative permeabilities considering both, oil viscosity depending on pressure via Eq. (5) and the case of viscosity independent on pressure, i.e., $\mu = \mu_{ob}$. The later case is shown, to compare the results with other authors such as Tang and Firoozabadi (2003), who disregarded the dependence of oil viscosity with pressure. Maini and Sarma (1994) did not report the oil relative permeability curve derived from their experiment. Andarcia et al. (2002) suggested oil relative permeability curves via Corey correlation: $kr_o = kr_o^{max}((1 - Sg - So_r)^e/(1 - So_r - Sg_c))$, considering $So_r = 0.87$ and $So_r = 0.83$ for the 2%-clay and 5%-clay experiments, respectively, $kr_o^{max} = 1$ and $Sg_c = 0$. They stated that relative permeability values larger than one are obtained from their data, but they dismiss the finding based on possible errors in the pressure transducers. Based on this and considering the effect of insufficient control of temperature in this experiment, we calculate the oil relative permeability considering three constant ΔP values (Fig. 7). First: a ΔP given by the average of all measured ΔPs; second: a ΔP given by the maximum recorded value and third: a ΔP given by the minimum recorded value. The gap between the curves corresponding to the last two cases represents the uncertainty that such fluctuations of pressure drop produce on the relative permeability. Fig. 7 evidences that though the uncertainty is large; the curve closest to the conventional behavior (obtained for the maximum ΔP) is still evidencing oil relative permeabilities larger than one. Thus, the analysis of relative permeability curves obtained from all experiments here discussed indicates that oil relative permeability values larger than one can be obtained. This indicates that other flow mechanisms ignored in the Darcian formalism could be taking place in this type of systems.

Non-smooth curves are obtained in all cases (Fig. 6). The abrupt changes are in most cases not associated to the fluctuations in differential pressure previously analyzed since the average curve we considered for our calculations reduces these effects. Nevertheless, depending on the time scale of existence of non-uniform bubble distributions relative to the period of time between consecutive measurements, the average curve could be affected by fluctuations. In the Tang and Firoozabadi (2003) case, there was not relation among the jumps in the relative permeability curves (Fig. 6a) and the fluctuations of differential pressure. For the curves obtained from Maini and Sarma (1994), abrupt

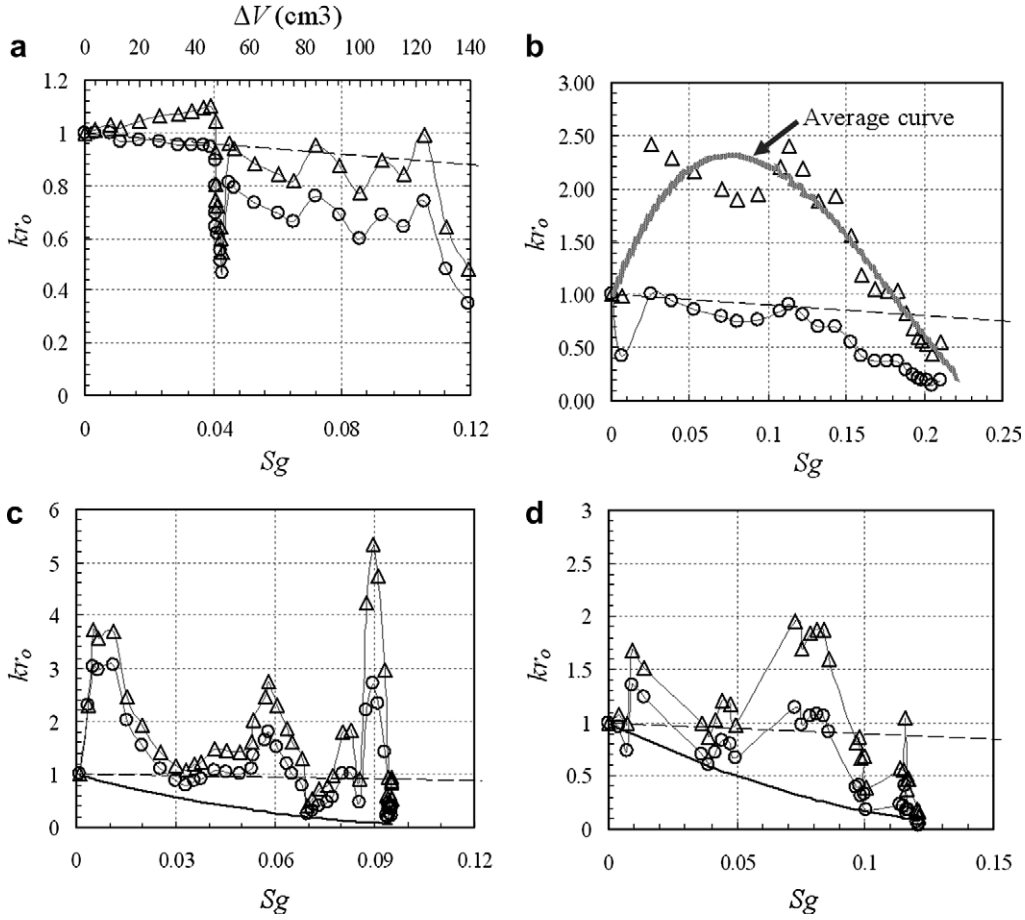

Fig. 6. Oil relative permeabilities obtained from: (a) Tang and Firoozabadi (2003); (b) Maini and Sarma (1994); (c) Andarcia et al. (2002), 2% of clay and (d) Andarcia et al. (2002), 5% of clay. In (c) and (d), the continuous line correspond to a Corey correlation, with exponent $e = 2.1$, suggested by the authors. Dashed line represents the miscibility curve ($kr_o = 1 - S_g$), triangles represent values obtained considering the viscosity varying with pressure by Eq. (5) and circles represent those obtained considering $\mu = \mu_{ob}$. Continuous gray lines are only a visual guide to make clearer the data trend.

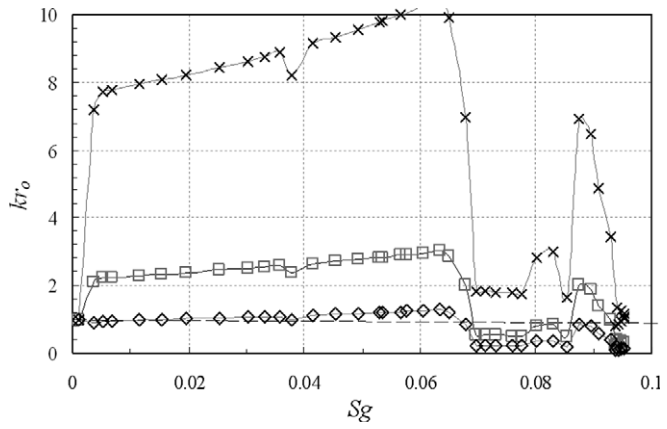

Fig. 7. Oil relative permeability curves obtained from Andarcia et al. (2002) reported data, assuming a constant differential pressure during the experiment. (□) an average ΔP; (◇) a maximum ΔP; (×) a minimum ΔP.

changes as those seen in the other cases were not observed (Fig. 6b) and the relatively smooth variations observed are correlated to changes in the flow regime evidenced by changes in capillary number. In the case of Andarcia et al. (2002) there is a correlation between some jumps in the relative permeability curves (Fig. 6c and d) and the variation of the average differential pressure. The average differential pressure curve that we considered in this case corresponds to the one reported by the authors in their Fig. 4, which is similar to the curve proposed by Tang and Firoozabadi (2003) is masking the fluctuations observed at time scales much smaller than the time scale of the entire experiment (see Fig. 14 of Andarcia et al. (2002)).

The curves obtained for the three constant ΔP values (Fig. 7) represent the behavior of relative permeabilities independent of the fluctuation of pressure drop in the Andarcia et al. (2002) experiments; however, the non-conventional behavior of the curves including some "jumps" prevails. Such jumps in relative permeabilities were also obtained through pore network simulations in previous work (Bravo et al., 2007) and their correlation with connectivity events was demonstrated. Conversely, in Tang and Firoozabadi (2003) experiment, the first very abrupt decrease of relative permeability occurred at around 4% of gas saturation and similarly, in Andarcia et al. (2002) experiments at about 7% of gas saturation. This similarity is in correspondence with the similarity of capillary numbers used in both experiments.

3. Simulations analysis

From the set of experiments previously discussed, oil relative permeability values larger than one were indeed observed. Previous work, based on pore network modeling, has shown that relative permeabilities larger than one can be due to the contribution of viscous coupling (Bravo et al., 2007), however, further studies need to done in order to explain the differences among the relative permeability curves obtained from experiments (Fig. 6). In this sense, we perform a set of simulations through pore network modeling considering different capillary numbers, which turns out to be one of the most important parameters controlling the flow dynamics, especially for the transport of a disconnected phase in porous media (Constantinides and Payatakes, 1991).

A two dimensional pore network model built on a regular square lattice was used in this study. The nodes are considered as having zero volume and the pressure drop and fluid storage occurs inside cylindrical capillaries, which have equal length and randomly distributed radius. A piston like gas–oil interface, characterized by an interfacial tension (γ) and equilibrium contact angle (θ) controls the coexistence of the two fluids inside each capillary. The fluids, described by their density and viscosity, are considered incompressible. The gas phase is composed of a monodisperse bubble distribution and the total number of bubbles (uniformly distributed in the network) is determined by the gas saturation. To reach the desired bubble size for each simulation step, two interfaces are set in the randomly selected location of each bubble. Both interfaces are moved and when any of them reaches a node, it is splitted in a number of new interfaces in all the neighboring capillaries. Poisseuille law is used to calculate the average velocity for single-phase flow in a capillary and for one or more interfaces in a capillary, the Poiseuille law is used in each single-phase region, while the capillary pressure gives the difference in hydrostatic pressure across the interface. Further description of the pore network simulator here used is given in Bravo et al. (2007) while the parameters involved in the simulations presented below are summarized in Table 2.

The pore network simulation model assumes that nucleation, growth, coalescence and breakup bubble phenomena occur in such a way that a near uniform and monodispersed bubble distribution is preserved at the time scales of the flow (Bravo et al., 2007). This assumption facilitates the study of the bubble size effect and gas saturation separately as well as it reduces the number of parameters needed if using typical pore network modeling (quasi-static

Table 2
Simulation parameters

Parameter	Values
Network size, nodes	50×50
Coordination number	4
Capillary lengths (l_c), mm	1
Average capillary radius ($\bar{r}$), μm	100
Range of capillary radii, μm	50–150
Oil viscosity (μ_o), Pa s	0.89
Oil density (ρ_o), kg/m^3	10^3
Gas viscosity (μ_g), Pa s	11.6×10^{-6}
Gas density (ρ_g), kg/m^3	0.663
Bubbles dimensions (l_b)	0.3, 1, 3, 10, 30, 100
Contact angle (θ),°	0
Interfacial tension (γ), N/m	40×10^{-3}
Gas bubble shape	Circular
Pressure difference (ΔP), N/m^2	10^5, 3×10^4, 10^4, 3×10^3, 10^3, 10^2

and dynamic); however, the simulations will not reflect experimental results unless this condition is satisfied and values of Table 2 are representative of the fluids, porous medium and rock–fluid interactions in the particular experiment. Visualization experiments performed under viscous flow regime (Lago et al., 2002 and Firoozabadi and Aronson, 1999) have evidenced that the aforementioned condition is approximately satisfied for time periods comparable to the time scales of flow (which typically is much smaller than the duration of the experiment); however, we do not pursuit reproducing a specific experiment, but complement the analysis of the behavior of relative permeabilities when disconnected bubbles, such as those observed during depressurization experiments, are in the porous space. Thus, the values of Table 2 just represent a characteristic hypothetical case of fluids and porous media typically used in depressurization experiments.

3.1. From viscous to capillary flow regime

One of the main factors determining the behavior of multiphase flow in porous media is the balance between capillary and viscous forces. This balance determines the flow regime that governs the dynamics of fluids, and consequently the features that should be captured in the transport equations. To evaluate the impact of the flow regime in the anomalous behavior evidenced in the previous section we perform simulations at six values of pressure gradient that cover a range of three orders of magnitude. Consequently a wide range of capillary numbers, calculated by Eq. (8) using the data offered in Table 2 is evaluated. The capillary pressure is estimated for the average capillary radius ($\bar{r}$) through Eq. (1).

In the simulations, while the pressure gradient, imposed to the network, decreased, more bubbles moving contrary to the flow direction were observed. The observation of pressure maps evidenced locally adverse pressure gradient in the region occupied by such bubbles due to a local predominance of capillary pressure. Fig. 8a shows a gas saturation map for $S_g \cong 0.04$ and bubble length $l_b \cong 30$ (given by the ratio of the bubble diameter to the average pore diameter). Bubbles' velocities (calculated as the average flow rate through the capillaries occupied by the bubble divided by the average capillary cross section) indicated some of them are moving contrary to the flow at network scale. Fig. 8b illustrates the pressure distribution in the region occupied by one of these bubbles when a pressure drop of 1.034 kPa ($Ca = 0.025$) is imposed to the pore network. Notice the adverse pressure gradient at local scale in this figure and observe the consequent flow rate in the x-direction plotted in Fig. 8c. Thus, bubbles motion is strongly related to the flow regime (viscous or capillary) at local level, and the evolution of the bubble velocity distribution during the transition between both regimes would allow to identify the critical capillary number (Ca_c) at the macroscopic scale, as the number where the average bubble velocity is zero. Fig. 9 illustrates how the bubble velocity distributions obtained for two different bubble sizes and two gas saturation values change with the capillary number (Ca).

It is seen in Fig. 9 that for $Ca \geqslant 0.82$ all the bubbles have positive velocity, which means that they move governed by the pressure gradient as in a viscous flow regime. For $Ca \leqslant 0.25$ a bi-modal distribution emerges and for $Ca = 2.5 \times 10^{-3}$ such bi-modal distribution evidences that the number of bubbles moving in the direction of

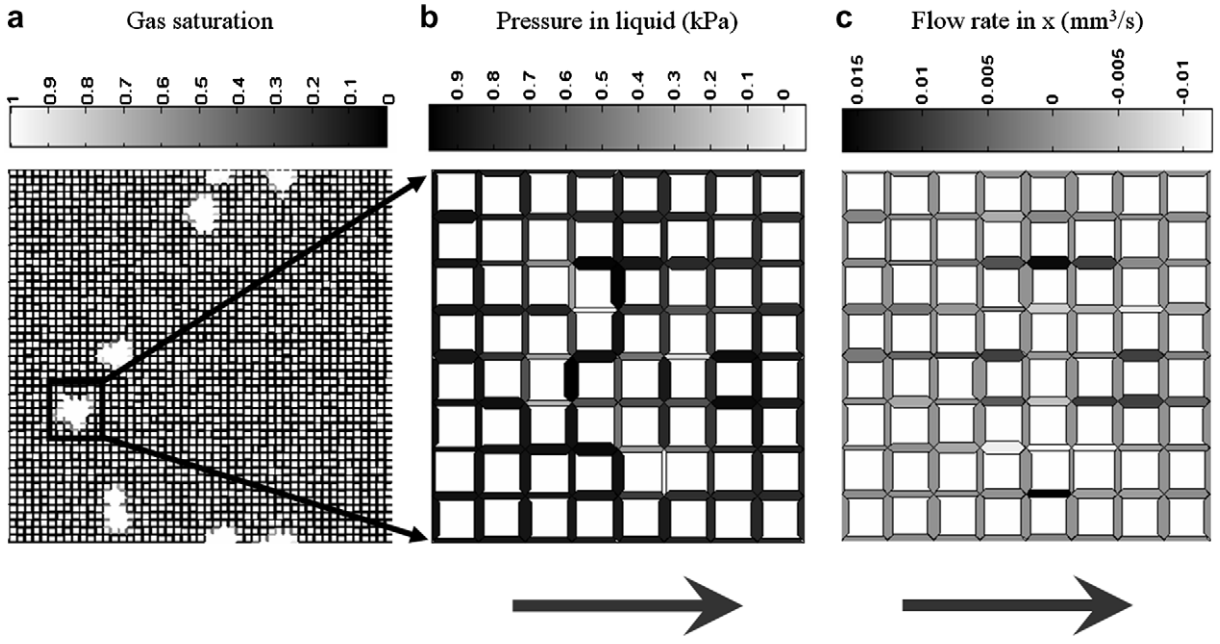

Fig. 8. (a) Gas distribution in the pore network for $S_g \cong 0.04$ and $l_b \cong 30$. Average gas saturation is plotted in those capillaries where both phases (gas and oil) are present. (b) Pressure in oil phase given by $P_o = P_g - Pc$. (c) Flow rate in x direction. In (b) and (c) just a zoom of the region corresponding to a bubble is illustrated. Arrows bellow these maps show the directions of macroscopic pressure gradient and flow.

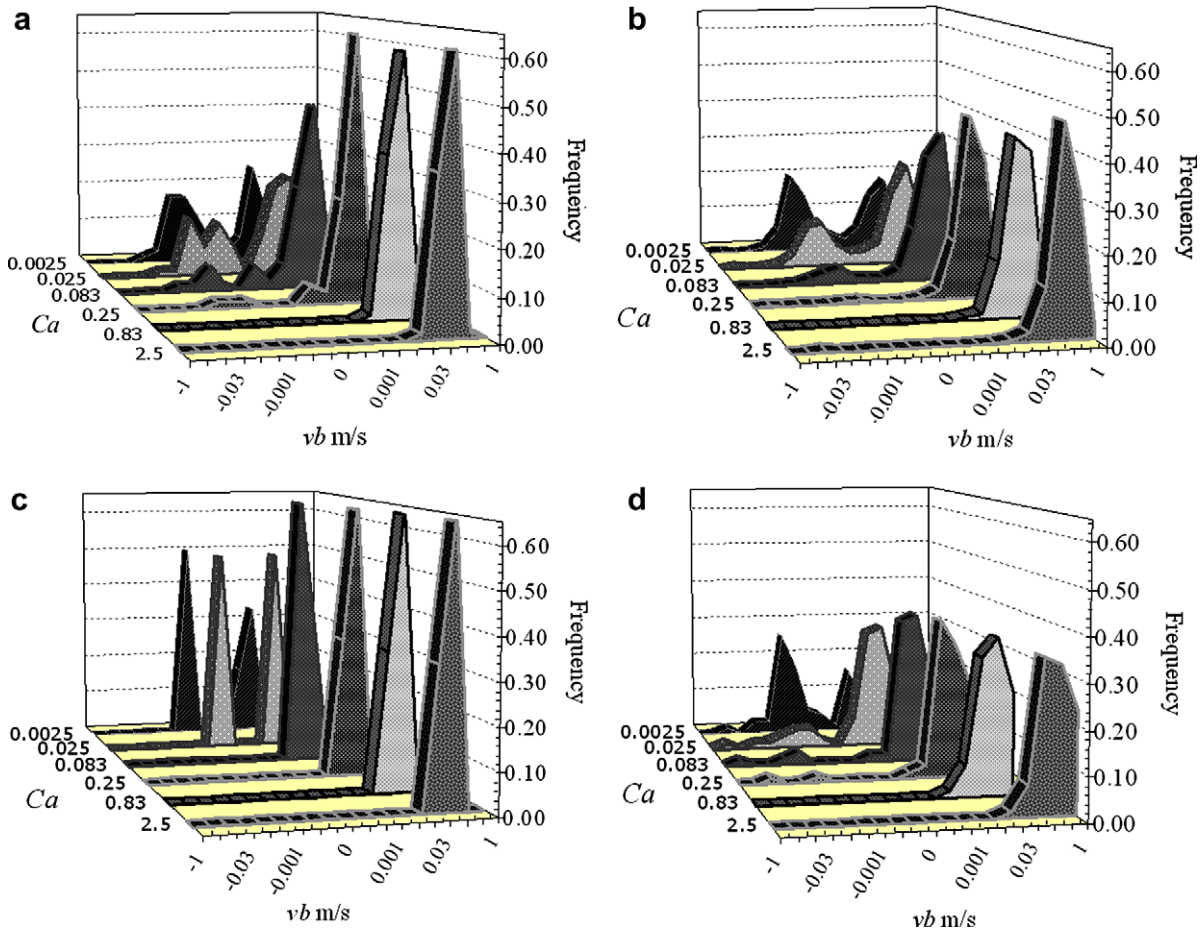

Fig. 9. Gas Bubble velocity distributions for six different flow conditions represented by the capillary number, obtained from Eq. 8 and six macroscopic pressure gradients imposed to the pore network (Table 2). (a) $l_b = 3$ and $S_g \cong 0.04$, (b) $l_b = 3$ and $S_g \cong 0.40$, (c) $l_b = 30$ and $S_g \cong 0.04$ and (d) $l_b = 30$ and $S_g \cong 0.40$.

macroscopic pressure gradient is approximately equal to the number moving in the opposite direction. For the bubble sizes and gas saturations studied in Fig. 9, the critical capillary number, Ca_c, can be located in the range from 10^{-2} to 10^{-3}. Thus, around these values the flow regime would suffer a transition from predominantly viscous to predominantly capillary or vice verse.

With this in mind, let us go back to the experimentally derived relative permeabilities, shown in Fig. 5. According to our previous analysis, it can be said that Maini and Sarma (1994) experiment was performed under a viscous flow regime that went from completely viscous, at the beginning of the test, to predominantly viscous at the end of the test. However, the experiment of Tang and Firoozabadi (2003) occurred under a predominantly viscous flow regime as well as the tests of Andarcia et al. (2002) whose behavior is observed to be more unstable. This result is in agreement with the differences of behavior observed in the relative permeability curves derived from these experiments (see Fig. 6).

The curves obtained from the Maini and Sarma (1994) experiment show particular features not observed in other experiments. Primarily, the absence of abrupt changes in the curve (Fig. 6b) is in correspondence with the minimum probability of connectivity events in a completely viscous flow regime, and the considerably improved probability of break up events (Lago et al., 2002). Secondly, values larger than one are present up to gas saturation of 18 %, just the value where the capillary number indicates that a transition from completely to predominantly viscous flow regime sets in.

3.2. Oil relative permeability

To complement the previous analysis, we obtain relative permeability curves using pore network simulations. Eq. (6) allows to calculate the oil relative permeabilities according to the Darcean approach, which are apparent values considering that the conventional Darcean formulation for two-phase flow neglects the contribution of viscous coupling explicitly captured in the generalized flow equations (Kalaydjian, 1990)

$$v_o = \frac{k \cdot kr_o}{\mu_o}(-\nabla p_o) + \frac{k \cdot k_{go}}{\mu_g}(-\nabla p_g) \tag{9}$$

$$v_g = \frac{k \cdot kr_g}{\mu_g}(-\nabla p_g) + \frac{k \cdot k_{og}}{\mu_o}(-\nabla p_o) \tag{10}$$

where k is the absolute permeability, kr_o and kr_g are the relative permeabilities to oil and gas, respectively and k_{go} and k_{og} are the corresponding coupling coefficient. Considering that there is not saturation gradient, the capillary pressure gradient is zero and consequently $\nabla P_o = \nabla P_g$. Thus, Eqs. (9) and (10) can be rewritten as

$$v_o = \frac{k \cdot kr_o^{ap}}{\mu_o}(-\nabla p_o) \tag{11}$$

$$v_g = \frac{k \cdot kr_g^{ap}}{\mu_g}(-\nabla p_o) \tag{12}$$

with apparent relative permeabilities given by

$$kr_g^{ap} = kr_g + \frac{\mu_g}{\mu_o}k_{og} = kr_g\left(1 + \frac{\mu_g}{\mu_o}\frac{k_{og}}{kr_g}\right) \tag{13}$$

$$kr_o^{ap} = kr_o + \frac{\mu_o}{\mu_g}k_{go} = kr_o\left(1 + \frac{\mu_o}{\mu_g}\frac{k_{go}}{kr_o}\right) \tag{14}$$

Eqs. (13) and (14) indicate that in principle apparent relative permeabilities larger than one can be obtained. However, the physics behind the curves' behavior is rigorously described if the viscous coupling and relative permeability terms are considered separately in the flow equations as in the generalized flow equations. Thus, the four transport coefficients are obtained in our simulations following the method proposed by Rose (1988), based on the difference that liquid and gas densities generates on pressure gradient, when the flow is parallel and perpendicular to the gravity.

According to Rose (1988), Eqs (9) and (10) are written for both flow conditions, hence four, instead of two, equations are available to derive the four transport coefficients. The equations are

$$q_o^{\perp} = kA\left(-\frac{kr_o}{\mu_o}\frac{\Delta p_o}{L} - \frac{k_{go}}{\mu_g}\frac{\Delta p_g}{L}\right) \tag{15}$$

$$q_g^{\perp} = kA\left(-\frac{kr_g}{\mu_g}\frac{\Delta p_g}{L} - \frac{k_{og}}{\mu_o}\frac{\Delta p_o}{L}\right) \tag{16}$$

$$q_o^{//} = kA\left(-\frac{kr_o}{\mu_o}\left(\frac{\Delta p_o}{L} - \rho_o g\right) - \frac{k_{go}}{\mu_g}\left(\frac{\Delta p_g}{L} - \rho_g g\right)\right) \tag{17}$$

$$q_g^{//} = kA\left(-\frac{kr_g}{\mu_g}\left(\frac{\Delta p_g}{L} - \rho_g g\right) - \frac{k_{og}}{\mu_o}\left(\frac{\Delta p_o}{L} - \rho_o g\right)\right) \tag{18}$$

Here, $q^{\perp}$ and $q^{//}$ represent the volumetric flow rate for perpendicular and parallel to gravity flow conditions, respectively. The product kA is determined by solving the single-phase case, where according to Darcy's law $q = (kA/\mu)(\Delta p/L)$. Eqs. (15)–(18) constitute the system of equations from where we obtain the four transport coefficients considering again that $\Delta p_o = \Delta p_g$ and the data summarized in Table 2.

Fig. 10a and b show the apparent oil relative permeability curves obtained via pore network simulations for $Ca = 0.25$ and $Ca = 0.025$, respectively. Fig. 10c and d illustrate the oil relative permeabilities, that do not contain the input of viscous coupling, for the same capillary num-

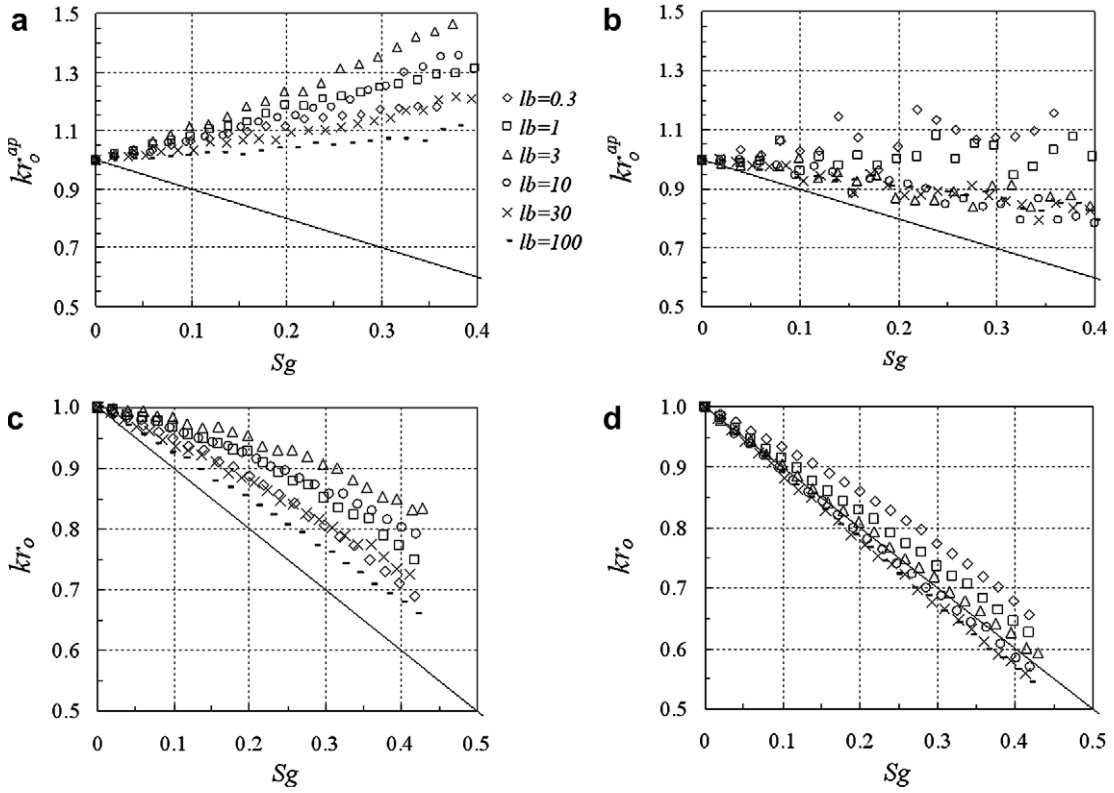

Fig. 10. (a) and (b) Apparent oil relative permeability curves obtained from conventional Darcean approach for $Ca = 0.25$ and $Ca = 0.025$, respectively. Oil relative permeability curves from generalized equations (Eqs. (15)–(18)) for: (c) $Ca = 0.25$ and (d) $Ca = 0.025$.

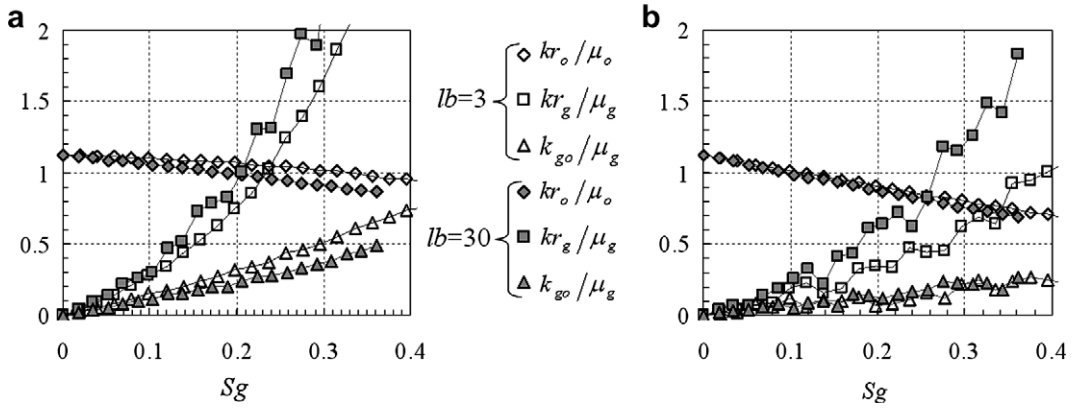

Fig. 11. Effect of capillary number and bubble sizes on the ratio of terms in Eqs. (9) and (10).

bers, respectively. Apparent relative permeabilities larger than one are observed in both, Fig. 10a and b, but this unusual behavior is considerably smaller in Fig. 10b and even unobserved for the three largest bubble sizes evaluated of 10, 30, and 100, respectively.

In general terms, according to Fig. 9, for a capillary number of 0.25 the dynamics occurs under a completely viscous flow regime while for 0.025 the regime is predominantly viscous, but capillary forces dominate more than 30% of bubbles velocities (Fig. 9d, which corresponds to $l_b = 30$ and $S_g = 0.4$, evidencing that capillary forces controlling less than 30% of bubbles). The physical consequences of the differences in flow regime at pore scale are known. In general as the capillary forces become more relevant, more bubble entrapment is expected (see Fig. 9). Macroscopic consequences are reflected in apparent oil relative permeability values smaller than those obtained for larger capillary numbers as observed comparing Fig. 10a and b.

Additionally, bubble growth and coalescence are favored respect to bubble break up when viscous forces lose dominance. Thus, when the gas saturation increases not only the number of bubbles can increase but also their size. Our simulator does not consider both ways of increasing the gas saturation at the same time, but we estimate the effect of bubble size on relative permeability by obtaining the curves for bubble sizes ranging from 0.3 to 100 times the capillary length. From these curves we can infer that for experiments where the flow regime range from completely to predominantly viscous, the oil relative permeability curve would reach the maximum for a considerably smaller gas saturation value due to the increase in bubble size and the decrease in capillary number effect, as in Maini and Sarma (1994) experiment.

Notice, that when the generalized formulation was considered and consequently both transport coefficients are separately studied, the relative permeability recovers its usual magnitude and no values larger than one exist in the curves of Fig. 10c and d. As a matter of fact, notice in Fig. 10d that for $l_b \geqslant 10$ the typical behaviors below of the miscibility line are obtained. This is basically because for $Ca = 0.025$ the predominantly viscous forces do not impede the effect of capillary forces on the bubble dynamics. On the other hand, relative permeabilities above the miscibility line, suggest that the oil phase have more porous space to flow than the porous space free of gas phase. This is a consequence of the fact that bubbles velocities are larger than the velocity of surrounding oil, thus gas is not obstructing the oil flow.

To evaluate the relative contribution of both terms, Darcean and viscous coupling on the volumetric flow rates given by the generalized Eqs. (9) and (10), plots of the weight or relative contribution of these terms, are offered in Fig. 11a and b for $Ca = 0.25$ and $Ca = 0.025$, respectively. Coupling terms satisfy the Onsager relation, i.e., $k_{go}/\mu_g = k_{og}/\mu_o$, thus only one of them is shown in the figure. It is observed that for the curves corresponding to oil, that larger bubble sizes imply smaller weight of both terms, being this effect less notable in Fig. 11b, where $Ca = 0.025$. From the comparison of Fig. 11a and b it is seen that the coupling term contribution to the volumetric oil rate is larger for $Ca = 0.25$ than for $Ca = 0.025$, and the contribution of both terms tend to be comparable as the gas saturation increase.

4. Conclusions

"Anomalous" behavior of oil relative permeabilities can be observed if the conventional Darcean approach is used to calculate them. However, it is important to understand the physics behind such unconventional curves. In this sense relative permeability larger than one is physically acceptable only if we keep in mind that this is an apparent magnitude, given that in the Darcy equation for two-phase flow, the coupling between phases is explicitly ignored. If relative permeabilities were obtained through the generalized formulation, getting relative permeability larger than one would be physically unacceptable in the context of laminar flow conditions.

In this paper we compiled and analyzed experiments that generated apparent relative permeabilities larger than one. This behavior, not previously reported according to

our literature review, was demonstrated to be consequence of neglecting the contribution of momentum transfer between fluid phases in the Darcean approach for the description of the two-phase flow in porous media.

We related the fluctuations in the differential pressure with the gas bubble sizes and distribution and found a relation between the amplitude of fluctuations and the macroscopic capillary pressure.

The effect of the capillary number on the relative permeability curves was investigated and it can be concluded that depending on this number the contribution of viscous coupling could lead to apparent relative permeability values larger than one or not. Experimentalists should be aware of the capillary number value in their experiments. Apparent relative permeabilities larger than one could not be observed in experiments where the capillary number is small enough as to consider a capillary flow regime.

Acknowledgement

We would like to express our gratitude to Dr. Arjan Kamp for his contribution clarifying the experimental data. The authors also thank the reviewers for their insightful comments and suggestions.

References

Andarcia, L., Kamp, A.M., Huerta, M., Rojas, G., 2002. The effect of clay fraction on heavy oil depletion test. SPE International Thermal Operations and Heavy Oil Symposium and International Horizontal Well Technology Conference, SPE-78968.

Bachmat, Y., Bear, J., 1986. Macroscopic modeling of transport phenomena in porous media: the continuum approach. Transport Porous Med. 1, 213–240.

Bauget, F., Langevin, D., Lenormand, R., 2001. Dynamic surface properties of asphaltenes and resins at the oil–air interface. J. Colloid Interf. Sci. 239, 501–508.

Bear, J., 1988. Dynamics of Fluids in Porous Media. Dover Publications, Inc., NY.

Bravo, M.C., Araujo, M., Lago, M.E., 2007. Pore network modeling of two-phase flow in a liquid-(disconnected) gas system. Physica A 375, 1–17.

Bora, R., Maini, B., Chakma, A., 2000. Flow visualization studies of solution gas drive process in heavy oil reservoir with a glass micromodel. SPE-Res. Eval. Eng. 3, 224–229.

Chen, Z., 2006. Heavy Oil, Part I. SIAM – Society for Industrial and Applied Mathematics, News 39, April.

Chen, Li S., Keh, H.J., 1998. Hydrodynamic interactions of two freely suspended droplets in linear flow fields. J. Colloid Interf. Sci. 204, 66–76.

Constantinides, G.N., Payatakes, A.C., 1991. A theoretical model of collision and coalescence of ganglia in porous media. J. Colloid Interf. Sci. 141, 486–504.

Corey, A.T., 1994. Mechanics of Immiscible Fluid in Porous Media, Third ed. Water Resources Publication, Colorado.

Donaldson, E., Tiab, D., 2003. Petrophysics: Theory and Practice of Measuring Reservoir Rock and Fluid Properties, Second ed. Gulf Publishing.

Drew, D.A., Passman, S.L., 1999. Theory of Multi Component Fluids. Gulf Publishing, NY.

Dullien, F.A.L., 1992. Porous Media, Fluid Transport and Pore Structure, Second ed. Academic Press, San Diego.

Firoozabadi, A., Aronson, A., 1999. Visualization and measurement of gas evolution and flow of heavy and light oil in porous media. SPE-Res. Eval. Eng. 2, 550–557.

Firoozabadi, A., Kashchiev, D., 1996. Pressure and volume evolution during gas phase formation in solution gas drive process. SPE J. 1, 219–227.

Hilfer, R., 1996. Transport and relaxation phenomena in porous media. Adv. Chem. Phys. XCII, 299–425.

Jackson, R., 2000. The Dynamics of Fluidized Particles. Cambridge University Press, NY.

Joseph, D.D., Kamp, A.M., Bai, R., 2002. Modeling foamy oil flow in porous media. Int. J. Multiphase Flow 28, 1659–1686.

Kalaydjian, F., 1987. A macroscopic description of multiphase flow in porous media involving spacetime evolution of fluid–fluid interface. Transport Porous Med. 2, 537–552.

Kalaydjian, F., 1990. Origin and quantification of coupling between relative permeabilities for two-phase flows in porous media. Transport Porous Med. 5, 215–229.

Karpyn, Z.T., Grader, A.S., Halleck, P.M., 2007. Visualization of fluid occupancy in a rough fracture using micro-tomography. J. Colloid Interf. Sci. 307, 181–187.

Khan, S.A., Al-Marhoun, M.A., Duffua, A.O. and Abu-Khamsin, S.A., 1987. Viscosity correlation for Saudi Arabian crude oil, SPE#15720.

Lago, M.E., Huerta, M., Gomes, R., 2002. Visualization study during depletion experiments of Venezuelan heavy oils using glass micromodels. J. Can. Petrol. Technol. 41, 41–47.

Lara, A., 1998. Study of interfacial behavior of oil–gas systems as function of pressure and its relation with stability of oleic foams. Thesis, Escuela de Química, UCV, Caracas.

Lyklema, J., 1991. In: Fund. Interf. Colloid Sci., vol. I. Academic Press, London.

Maini, B.B., Sarma, H., 1994. Role of non-polar foams in production of heavy oils. Adv. Chem. Series 242, 405–420.

McDougall, S., Sorbie, K., 1999. Estimation of critical gas saturation during pressure depletion in virgin and waterflooded reservoirs. Petrol. Geosci. 5, 229–233.

Perunicic, M., Babin, M., 2001. On the local porosity of the regularly packed spherical mono-dispersed particles. Bull. Chem. Technol. Macedonia 20, 77–82.

Rose, W., 1988. Measuring transport coefficients necessary for the description of coupled two-phase flow of immiscible fluids in porous media. Transport Porous Med. 3, 163–171.

Sahimi, M., 1993. Flow phenomena in rocks: from continuum models to fractals, percolation, cellular automata, and simulated annealing. Rev. Modern Phys. 65, 1393–1534.

Tang, G-Q., Firoozabadi, A., 2003. Gas and liquid phase relative permeabilities for cold production from heavy oil reservoirs. SPE-Res. Eval. Eng., 70–80.

Tang, G.-Q., Sahni, A., Gadelle, F., Kumar, M., Kovscek, A.R., 2006. Heavy-oil solution gas drive in consolidated and unconsolidated rocks. SPE J., 259–268.

Vizika, O., Avraam, D.G., Payatakes, A.C., 1994. On the role of the viscosity ratio during low capillary number forced imbibition in porous media. J. Colloid Interf. Sci. 165, 386–401.

Whitaker, S., 1986a. Flow in porous media I: a theoretical derivation of Darcy's law. Transport Porous Med. 1, 3–25.

Whitaker, S., 1986b. Flow in porous media II: the governing equations for immiscible, two-phase flow. Transport Porous Med. 1, 105–125.